Supporting Information

for

Doping with Graphitic Nitrogen Triggers Ferromagnetism in Graphene

Piotr Błoński,[†] Jiří Tuček,[†] Zdeněk Sofer,[§] Vlastimil Mazánek,[§] Martin Petr,[†] Martin Pumera,[‡] Michal Otyepka,[†] and Radek Zbořil[†,*]

[†] Regional Centre of Advanced Technologies and Materials, Department of Physical Chemistry, Faculty of Science, Palacký University in Olomouc, 17. listopadu 1192/12, 771 46 Olomouc, Czech Republic.

[§] Department of Inorganic Chemistry, University of Chemistry and Technology Prague, Technická 5, 166 28 Prague 6, Czech Republic.

[‡] Division of Chemistry & Biological Chemistry, School of Physical and Mathematical Sciences, Nanyang Technological University, 637371 Singapore.

* Corresponding authors: Phone: +420 585634337, Fax: +420 585634761, E-mail address: radek.zboril@upol.cz (Radek Zbořil); Phone: +420 585634764, Fax: +420 585634761, E-mail address: michal.otyepka@upol.cz (Michal Otyepka).

Number of figures: 11

Number of tables: 4

Number of pages: 10

Supporting Figures

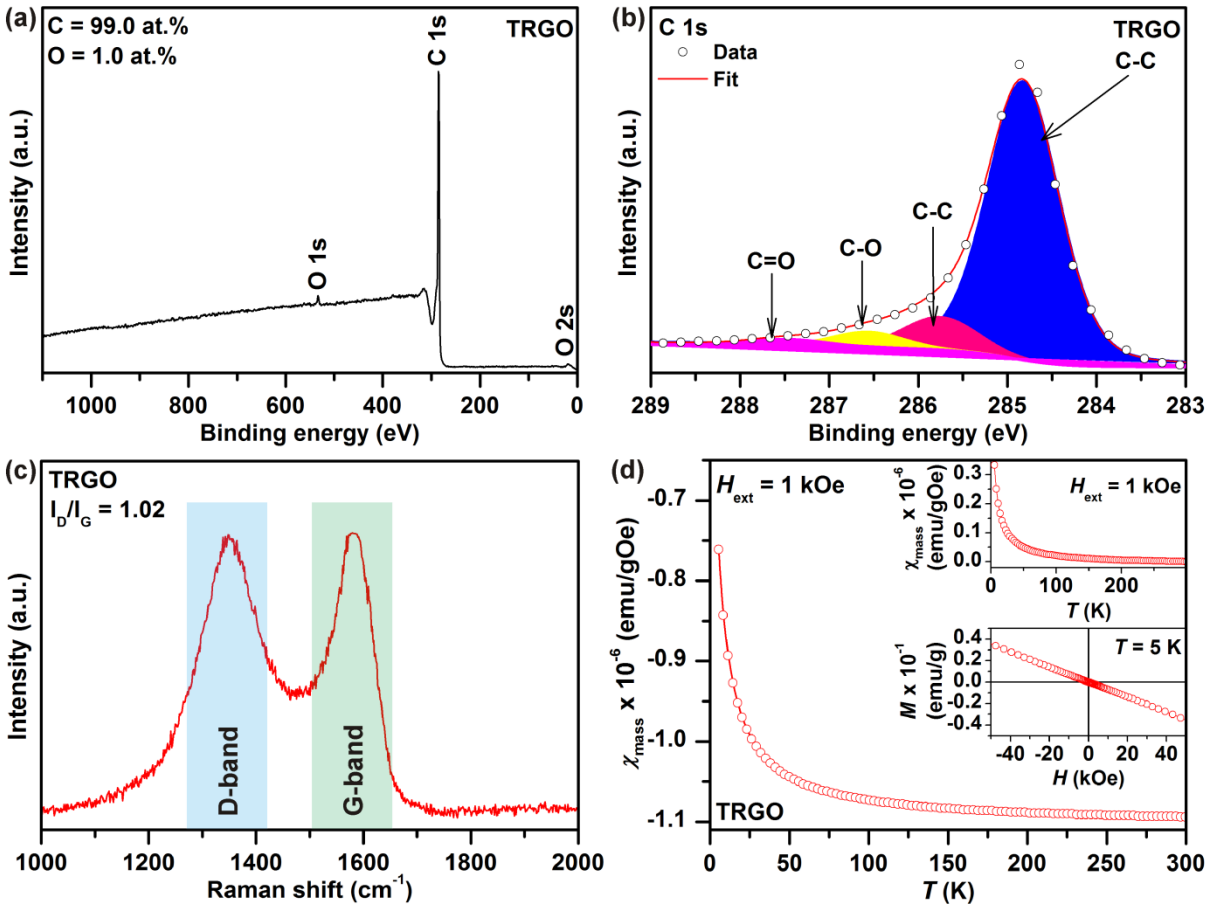

Figure S1. (a) Survey and (b) high-resolution C 1s XPS pattern of the TRGO sample with the peaks belonging to C and O and various bonds indicated. (c) Raman spectrum of the TRGO sample with the D-band, G-band, and I_D/I_G ratio indicated. (d) Temperature evolution of the mass magnetic susceptibility, χ_{mass}, of the TRGO sample measured under an external magnetic field of 1 kOe. The insets show the temperature profile of χ_{mass} after the subtraction of the diamagnetic component and behavior of 5 K hysteresis loop of the TRGO sample.

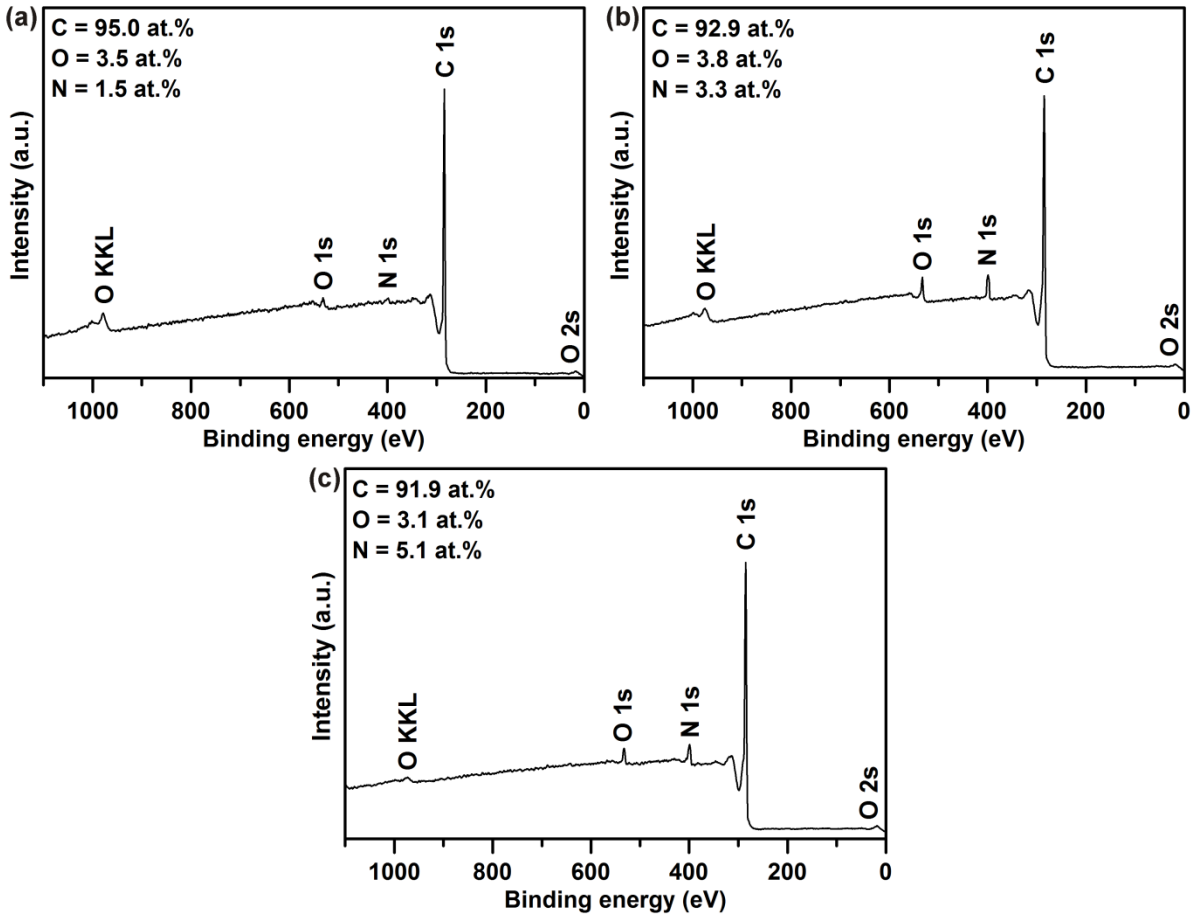

Figure S2. Survey XPS pattern of the (a) $GN_{0.015}$, (b) $GN_{0.033}$, and (c) $GN_{0.051}$ sample with the peaks belonging to C, N, and O indicated.

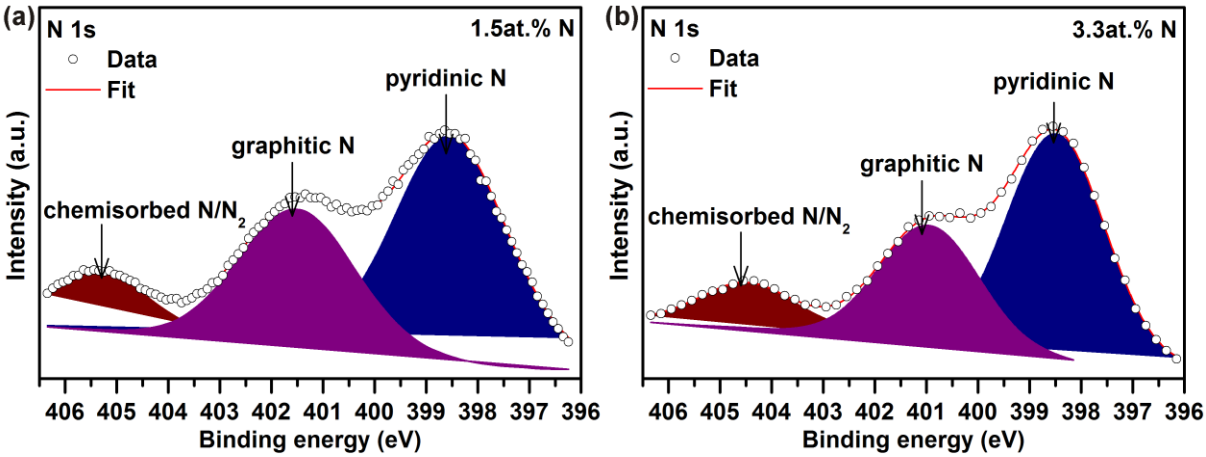

Figure S3. High-resolution N 1s XPS pattern of the (a) $GN_{0.015}$ and (b) $GN_{0.033}$ sample with the peaks belonging to differently coordinated nitrogen indicated.

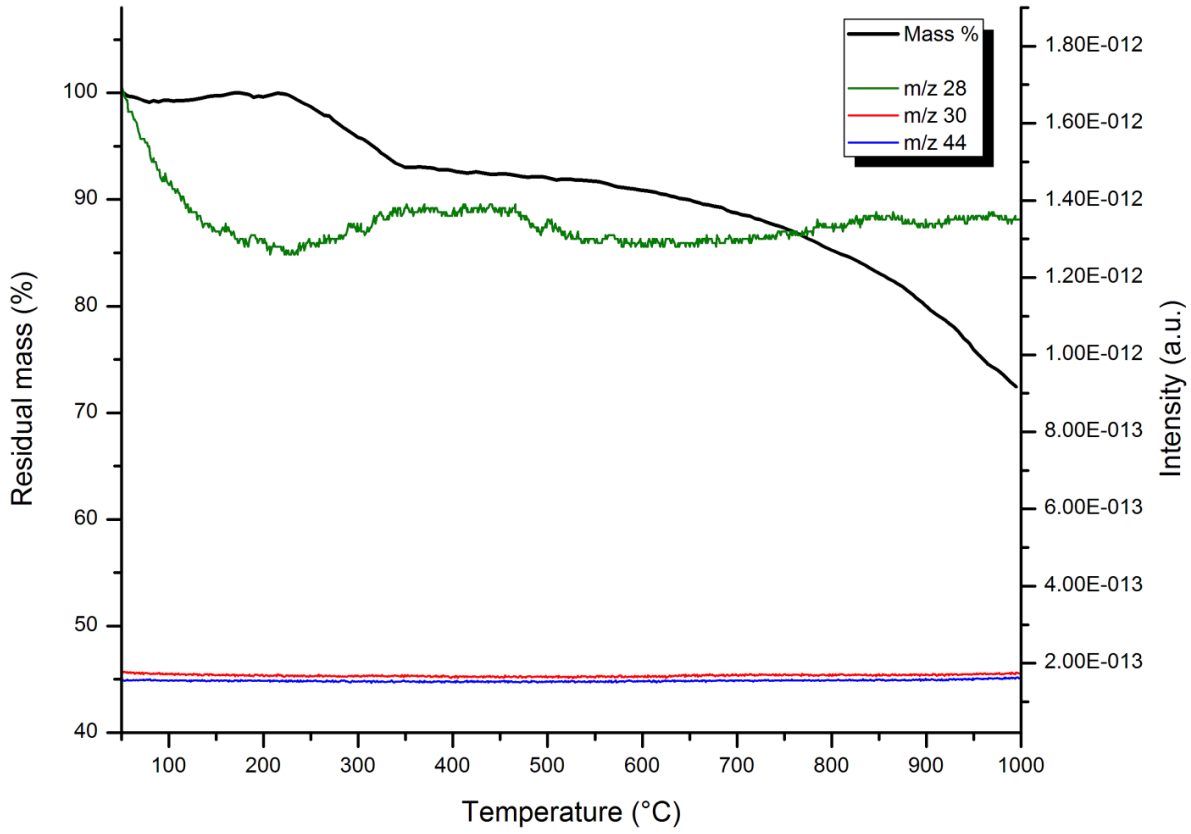

Figure S4. Thermogravimetric (TG) and evolved gas analysis (EGA) measurements of the $GN_{0.051}$ sample with a continuous detection of the release of the fragments with m/z = 28, 30, and 46 corresponding to N/N_2, NO, and NO_2, respectively.

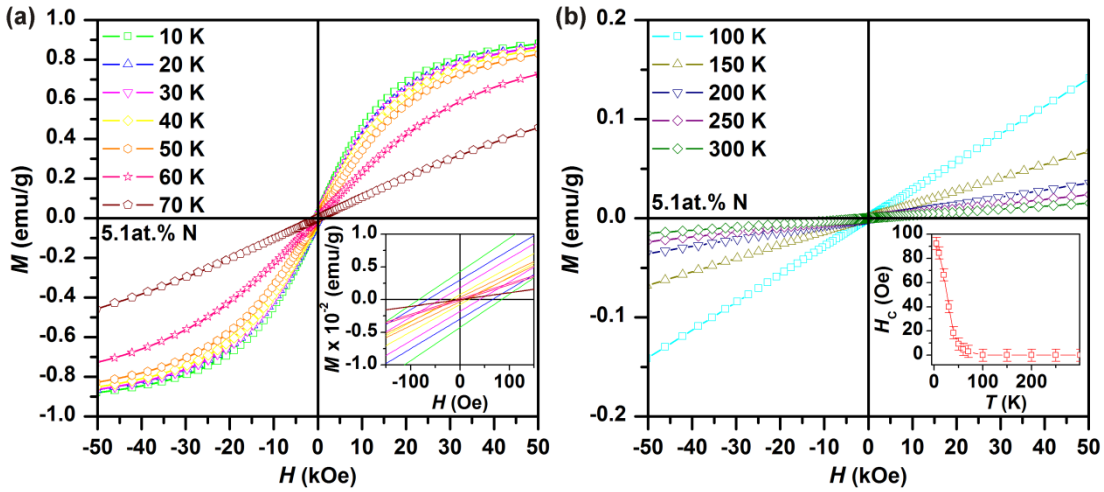

Figure S5. Hysteresis loops of the $GN_{0.051}$ sample, recorded in the temperature interval (a) from 10 to 70 K and (b) from 100 to 300 K. The inset in panel (a) shows the behavior of hysteresis loops around the origin. The inset in panel (b) shows the temperature evolution of coercivity, H_C, derived from the respective hysteresis loops of the $GN_{0.051}$ sample.

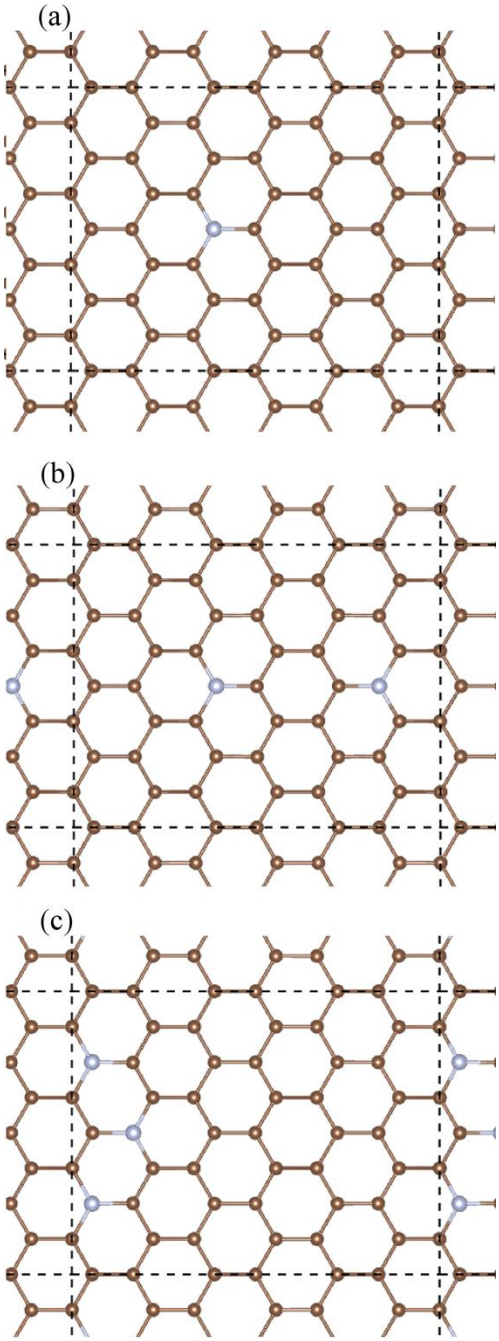

Figure S6. Top view of the nonmagnetic ground state structure doped by (a) 2.1, (b) 4.2, and (c) 6.25 at. % of graphitic nitrogen.

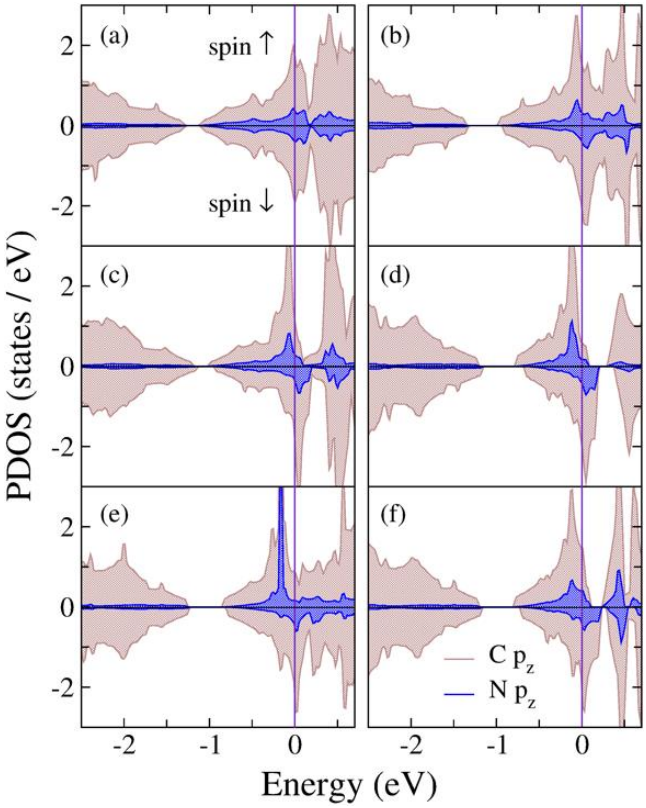

Figure S7. Partial densities of states calculated for N-doped graphene magnetic structures containing 6.25 at. % of nitrogen: (a) 0.1; (b) 0.4; (c) 0.7; (d) 0.8; (e) 0.4; and (f) 0.6 μ_B per supercell (*cf*. Figure 7).

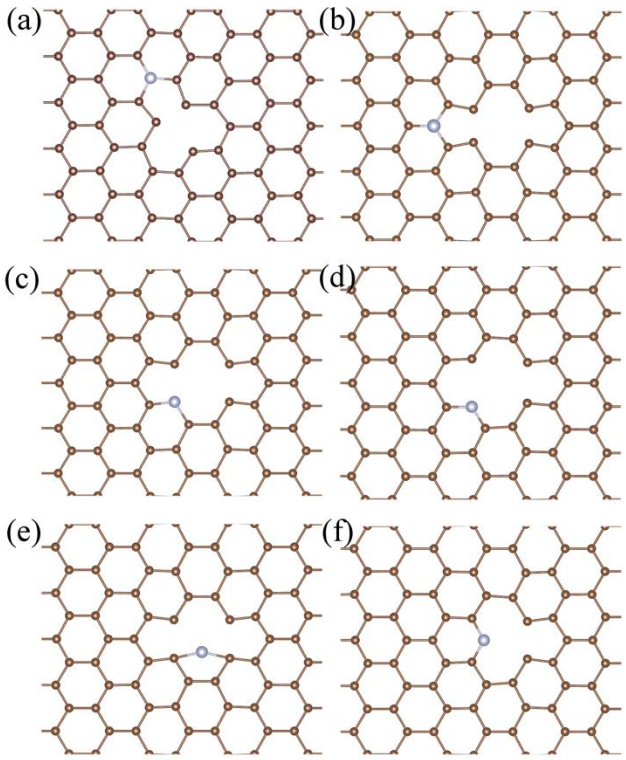

Figure S8. A single pyrrolic nitrogen in graphene inside the pentagonal ring in a vicinity of (a) single-vacancy (SV) and (b) di-vacancy (DV) defect. The carbon atoms near vacancy defects undergo an in-plane displacement leading to the formation of 5- and 9-membered rings (SV), while upon the reconstruction of the atomic positions neighboring to DV, two pentagons and one octagon defect appear. In the pentagonal rings, due to the reconstructed C–C bonds, the 2-fold-coordinated C atoms are not present. (c, d) 5-membered ring opening due to the substitution of one of the C atom participating in the reconstructed C–C bond with the nitrogen atom. Panels (c) and (d) show initial pyrrolic and final pyridinic N-structure, respectively. (e) Initial pyrrolic and (f) final pyridinic nitrogen inside the octagonal ring of the DV defect.

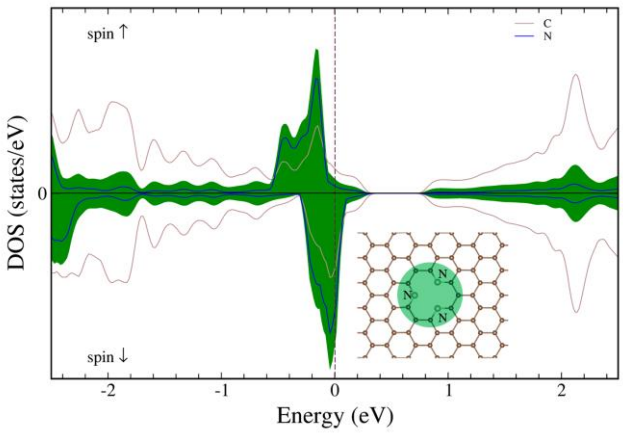

Figure S9. Densities of states (DOS) calculated for trimerized pyridinic nitrogen embedded in the graphene lattice (shown in the inset). DOS for atoms in the green circle are plotted in green.

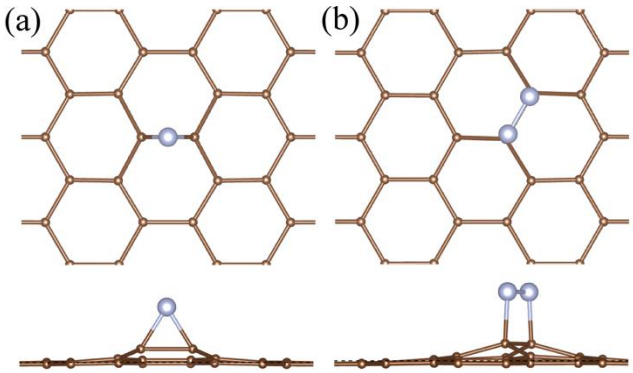

Figure S10. (a) Nitrogen adatom and (b) dimer in the most stable adsorption positions, i.e., the bridge site between the C atoms (E_{ad} = – 0.86 eV) and on-top of the C atoms (E_{ad} = – 2.96 eV/N), respectively.

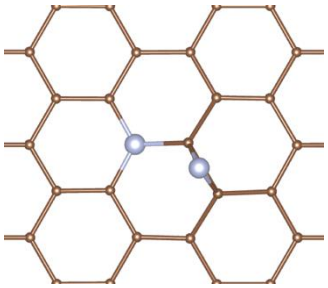

Figure S11. Nitrogen adatom near the graphitic nitrogen (E_{ad} = – 1.90 eV).

Supporting Tables

Table S1. Concentrations of the selected metals in the TRGO and N-doped samples, as determined by ICP-MS.

Sample	Cr (ppm)	Mn (ppm)	Fe (ppm)	Co (ppm)	Ni (ppm)	Zn (ppm)
TRGO	10.98	0.59	6.14	0.32	1.48	28.58
$GN_{0.015}$	11.12	0.85	5.74	0.21	1.65	27.14
$GN_{0.033}$	10.42	0.72	6.58	0.24	2.15	25.89
$GN_{0.051}$	9.58	0.48	5.20	0.30	1.98	28.89

Table S2. Atomic percentage (at.%) of C, N, and O in the TRGO, $GN_{0.015}$, $GN_{0.033}$, and $GN_{0.051}$ sample, derived from the analysis of the respective survey XPS patterns.

Sample	C (at.%)	N (at.%)	O (at.%)
TRGO	99.0	----	1.0
$GN_{0.015}$	95.0	3.5	1.5
$GN_{0.033}$	92.9	3.8	3.5
$GN_{0.051}$	91.9	3.1	5.1

Table S3. Fitting results of the high-resolution C 1s, O 1s, and N 1s XPS patterns recorded for the TRGO, $GN_{0.015}$, $GN_{0.033}$, and $GN_{0.051}$ sample, showing the presence of individual bonds identified as peaks in the high-resolution C 1s, O 1s, and N 1s XPS profiles and expressed in % of the total spectral area of all the spectral components found in a particular high-resolution XPS pattern.

Sample	C 1s				O 1s		N 1s		
	C-C (%)	C-N (%)	C-O (%)	C=O (%)	C-O (%)	C=O (%)	pyridinic N (%)	graphitic N (%)	chemisorbed N/N_2 (%)
TRGO	81	---	15	4	91	9	---	---	---
$GN_{0.015}$	76	10	10	4	95	5	57	31	12
$GN_{0.033}$	76	13	9	2	78	22	57	30	13
$GN_{0.051}$	73	16	9	2	63	37	55	31	14

Table S4. Formation energy, E_f (in eV), magnetic moment per cell (in μ_B), charge transfer (in electrons) to the dopant obtained from the Bader analysis, energy gap at the Dirac point (in meV) calculated as the mean value for spin-up and spin-down channels, and the shift of the Dirac point (in eV) with respect to the Fermi level calculated for different concentrations of nitrogen atoms in N-doped graphenes. Symbols in the brackets refer to the structures in Figure 6, Figure 7, and Figure S6 in Supporting Information.

Concentration	E_f	**Magnetic moment**	**Bader charge**	**Energy gap**	**Dirac-point shift**
2 at. % (S6a)	3.55	0.00	– 1.206	138	– 0.74
4 at. % (S6b)	3.51	0.00	2× – 1.214	39	– 1.01
4 at. % (6)	3.58	0.23	– 1.211 – 1.217	60	– 0.85
6 at. % (S6c)	3.56	0.00	2× – 1.206 – 1.235	99	– 0.95
6 at. % (7a)	3.70	0.08	2× – 1.187 – 1.212	129	– 1.19
6 at. % (7b)	3.73	0.44	2× – 1.193 – 1.199	358	– 1.15
6 at. % (7c)	3.78	0.71	3× – 1.187	160	– 1.07
6 at. % (7d)	3.81	0.81	2× – 1.201 – 1.211	437	– 0.95
6 at. % (7e)	3.81	0.44	2× – 1.192 – 1.182	414	– 1.04
6 at. % (7f)	3.86	0.61	2× –1.184 – 1.193	409	– 0.97